Crenelated fast oscillatory outputs of a two-delay electro-optic oscillator

Lionel Weicker and Thomas Erneux
Université Libre de Bruxelles, Optique Nonlinéaire Théorique, Campus Plaine, Code Postal 231, 1050 Bruxelles, Belgium

Maxime Jacquot, Yanne Chembo, and Laurent Larger
FEMTO-ST/Optics department, Unité Mixte de Recherche CNRS No.6174, University of Franche-Comté, 16 route de Gray, 25030 Besançon Cedex, France

(Received 23 June 2011; revised manuscript received 15 November 2011; published 7 February 2012)

An electro-optic oscillator subject to two distinct delayed feedbacks has been designed to develop pronounced broadband chaotic output. Its route to chaos starts with regular pulsating gigahertz oscillations that we investigate both experimentally and theoretically. Of particular physical interest are the transitions to various crenelated fast time-periodic oscillations, prior to the onset of chaotic regimes. The two-delay problem is described mathematically by two coupled delay-differential equations, which we analyze by using multiple-time-scale methods. We show that the interplay of a large delay and a relatively small delay is responsible for the onset of fast oscillations modulated by a slowly varying square-wave envelope. As the bifurcation parameter progressively increases, this envelope undergoes a sequence of bifurcations that corresponds to successive fixed points of a sine map.

DOI: 10.1103/PhysRevE.85.026206 PACS number(s): 05.45.−a, 42.65.Sf

I. INTRODUCTION

Nonlinear problems modeled by delay-differential equations have attracted much interest during the past two years [1–8]. A delay appears in any mechanical or physiological control system because time is needed to sense information and react to it. If this time lag is too important, oscillatory instabilities often may take place. These stability problems caused by a delay arise in all areas of science and engineering and are explored with different objectives and expectations. Mechanical engineers studying chatter instabilities in high-speed machining are first interested in determining the conditions for stable operation [1]. In nonlinear optics, however, regular and irregular oscillatory outputs caused by a delayed feedback are studied both experimentally and theoretically [9]. These instabilities are either undesired because they limit the performance of a particular device (e.g., for ultrapure microwave generation) or, in contrast, they are used to design practical systems such as high-frequency and broadband optical chaotic oscillators (e.g., for secure chaos communication [10] or high-speed random number generation [11]) or to develop alternative imaging techniques [9].

The introduction of a second delay in a single-delayed-feedback problem does not necessarily mean the emergence of more complex behaviors. For particular combinations of the two delays, the second feedback can be used to stabilize a previously unstable steady state or even a desired unstable periodic orbit [12]. While there is a substantial body of literature devoted to experimental studies of single-delayed-feedback problems, little has been attempted experimentally on two-delay problems [13–15]. In this paper we consider a broadband chaotic electro-optic oscillator (EOO) subject to two independent delayed feedbacks [16]. Standard EOOs typically incorporate a nonlinear (intensity) modulator, an optical-fiber delay line, and an optical detector in a closed-loop resonating configuration. This hybrid microwave source is capable of generating, within the same optoelectronic delayed-feedback topology, either an ultralow-jitter (low-phase-noise) single-tone microwave oscillation, as used in radar applications [17,18], or a broadband chaotic carrier typically intended for physical data encryption in high-bit-rate optical communications [19].

The dynamical behavior of the (nonstandard) EOO that we investigate here depends on a large delay T and a relatively small delay δT ($T/\delta T \sim 10^2$). The latter results from the unusual use of a phase modulator instead of an intensity one (as for the standard EOO). As we shall demonstrate experimentally and theoretically, these delays are responsible for a cascade of period-doubling bifurcations to multiperiodic regimes that depend on only two basic periods T_1 and T_2. Because $T/\delta T$ is large, we show that the ratio T_2/T_1 is close to a large integer value.

The paper is organized as follows. In Sec. II we describe the particular dual-delay experimental setup of concern and discuss three time traces obtained by gradually increasing its feedback gain. Of particular interest are their quite different temporal waveforms (see Fig. 1) exhibiting different physical time scales. This motivates the use of multiple-time-scale techniques for their theoretical description. In Secs. III and IV we formulate the model equations and determine the Hopf bifurcation points analytically. Their asymptotic properties in terms of the two delays are analyzed in Sec. V and motivate the construction of the first Hopf bifurcation branch. In Sec. VI we then apply the method of multiple time scales and determine second- and higher-order bifurcations. Our main results are summarized and discussed in Sec. VII.

II. ELECTRO-OPTIC PHASE DYNAMICS

We propose to investigate the electro-optic phase oscillator shown in Fig. 2. The phase modulator (PM) is fed by a cw-injected light (point 1) coming from a 50-mW telecom semiconductor distributed feedback laser. The optical phase of the injected light is then modulated according to the voltage $v(t)$ applied to the electrical rf input of the PM, while the intensity of the output light (point 2) remains constant. The

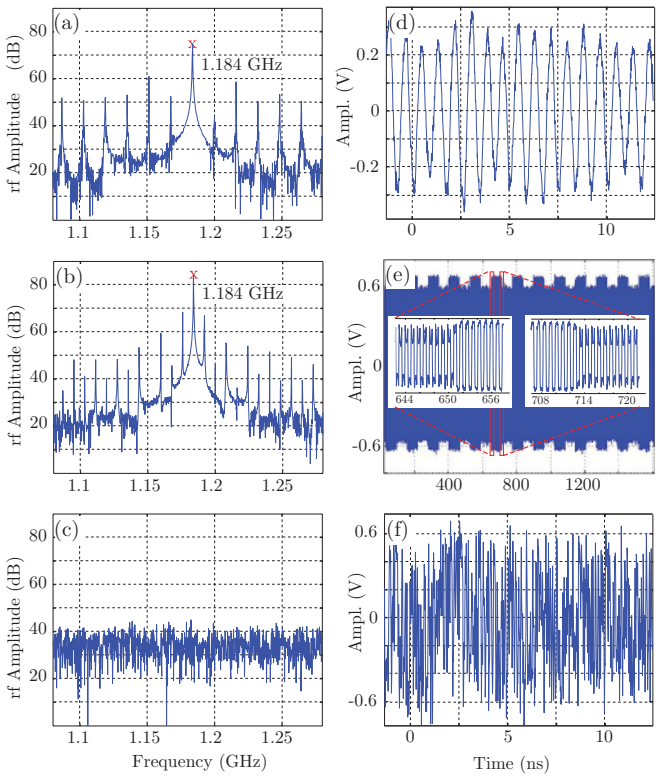

FIG. 1. (Color online) Experimental rf spectra (left) and time series (right) for different values of the feedback gain: (a) and (d) $\beta \simeq 0.5 = \beta_H$ [Hopf threshold, observed for an optical power measured at point 3 (see Fig. 2), which is used as a reference for the experimental calibration of the linear β scaling]; (b) and (e) $\beta \simeq 1.24$ (crenelated waveform, with the close-up showing the rising and falling edge of the envelope); and (c) and (f) $\beta \simeq 5.9$ (fully developed chaos).

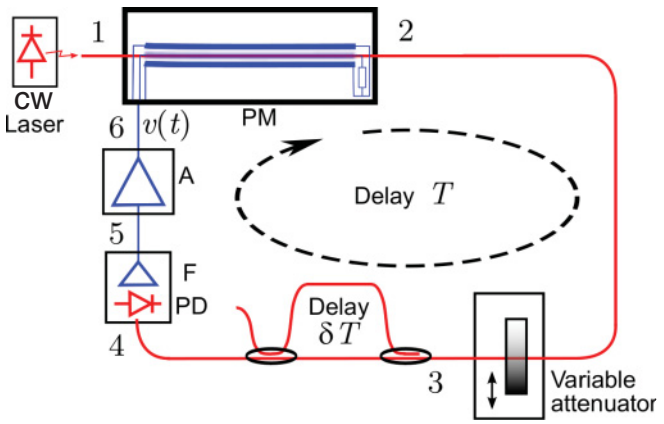

FIG. 2. (Color online) Experimental setup: 1, unmodulated light from a semiconductor laser, $E_1 = E_0 e^{i\omega_0 t}$; 2, constant intensity, but phase-modulated light by the electro-optic phase modulator PM, according to the rf voltage $v(t)$ delivered by the driver or amplifier A, $E_2 = E_0 e^{i[\omega_0 t + \phi(t)]}$, where $\phi \propto v$; 3, tuned optical intensity via a variable attenuator, $|E_3|^2 = \gamma |E_2|^2$, for adjusting the normalized feedback gain $\beta \propto \gamma$; 4, nonlinear, nonlocal, phase to amplitude conversion by a passive imbalanced Mach-Zehnder interferometer (imbalancing δT), $E_4 = 1/2[E_3 + (E_3)_{\delta T}]$; 5, optical intensity to voltage conversion by an amplified photodetector PD and dynamics limitation by the electronic bandpass filtering F; 6, amplification by a broadband Telecom driver, before applying the feedback to the PM; the total feedback delay T originates mainly from the optical devices (PM waveguide and fiber pigtails optical components) and partly from the electronics (small connectors and devices group delay).

output light intensity leaving the phase modulator is tuned by a variable optical attenuator, the resulting light intensity being measured at point 3 for the evaluation of the normalized and linearly dependent feedback loop gain β. The corresponding normalized gain β plays the role of the bifurcation parameter and can be interpreted as the weight for the dual-delay nonlinear feedback in the dynamics. The attenuated light then enters a fiber-based passive imbalanced interferometer (time imbalancing $\delta T \sim 402.68$ ps). This interferometer converts nonlinearly the input phase modulation into an output intensity modulation, which can then be detected by a photodiode at point 4. The electrical signal at the photodiode output is filtered according to the bandwidth of the electronic feedback (point 5) and amplified before being applied to the PM rf input (point 6). The serial combination of the few meters of fiber pigtails, the small electrical connections, and the various electrical group delay of rf devices result in a total time delay in the closed-loop oscillation measured to be $T \sim 61.89$ ns.

When the feedback gain is progressively increased from zero, fast oscillations are first observed if $\beta \gtrsim 1/2 = \beta_H$, as illustrated by the experimental spectrum and time trace in Figs. 1(a) and 1(d). This regime is recorded right after the first Hopf bifurcation point and serves as a reference point for the experimental calibration of the bifurcation parameter β calculated from the optical power measured at point 3. Right after this Hopf bifurcation, the oscillations are weakly stable and exhibit amplitude fluctuations. In the rf spectrum [fast Fourier transform (FFT) computed spectra with a sub-megahertz resolution, from 600 kSamples time traces recorded at a 8.3-ps sampling period with 120 GSamples/s Lecroy WaveMaster 845Zi], we clearly identify the regular oscillation frequency at $f_1 = 1.184$ GHz or, equivalently, a period $T_1 \simeq 0.845$ ns. This period is close to $2\delta T = 0.805$ ns, suggesting that only δT plays a role for the Hopf bifurcation. From the spectrum, we also note the small noisy peak modes attached to the large delay T, which is at the origin of the delay modes spaced by $1/T \simeq 16.16$ MHz. Their noisy character is revealed by the peak amplitude fluctuations in time (from one FFT to the next one), whereas the deterministic character of the dominating peak (at the oscillating frequency) leads to a much more stable peak height. For slightly larger values of β ($\beta \simeq 0.6$–0.9), the rf noisy amplitude fluctuations of the oscillation disappear and the signal shape progressively moves to a square wave with the same fundamental frequency.

The plot in Figs. 1(b) and 1(e) illustrates a situation observed when β is further increased and has passed a secondary bifurcation point near $\beta_C \simeq 1.14$ [from the measured optical power at point 3 in Fig. 2, the plot in Figs. 1(b) and 1(e) corresponds to a regime with $\beta \simeq 1.24$]. At this point, slowly varying crenelated fast periodic rf oscillations emerge. The period of the slow time envelope is $T_2 \simeq 122$ ns, which is close to $2T = 123.78$ ns, whereas the fast oscillations within the envelope still exhibit the faster period T_1. This suggests that both δT and T play an active role for the secondary bifurcation. The period of the slow-time envelope is observed in the FFT

spectrum by the sideband peaks at $\pm(2T)^{-1}$ surrounding the large dominant peak at $f_1 = 1/T_1$. These sideband peaks in the FFT spectrum are consistent with the time trace because of the amplitude modulation (AM) feature observed in the time series [Fig. 1(e)]. We also note that all peaks in the FFT spectrum [Fig. 1(b), the noisy ones far from the carrier, the carrier itself, and the main dominating AM sidebands] are regularly spaced by $1/2T$, thus exactly matching half of a large delay mode frequency, whereas the peak spacing in the FFT of Fig. 1(a) (right after the first Hopf bifurcation) matches $1/T$.

For much larger values of β, chaotic oscillations are typically observed. The broadband and very flat spectrum [Figs. 1(c) and 1(f), with an experimental β evaluated at about 5.9] covers actually the 12-GHz bandwidth of the electronic feedback [16], of interest, e.g., for spectral masking of a binary information signal at bit rates as fast as 10 Gbit/s [20].

Our main objective in this paper is to analyze the secondary- and higher-order bifurcations that immediately appear after the first Hopf bifurcation. As already anticipated in Ref. [16], the large number of bifurcations results from the interplay between two independent delays, namely, δT and T. We shall take advantage of the small ratio $\delta T/T$ and determine a two-time asymptotic approximation of the solution. To this end, we first determine the Hopf bifurcations of the basic steady state and obtain useful asymptotic expressions for the bifurcation point and its frequency. We then propose a nonlinear analysis where we derive equations for maps.

III. DUAL-DELAY DYNAMICAL MODEL

According to the setup in Fig. 2, we first derive the dynamical model of the dual-delay oscillator (see Ref. [16] for details). The nonlocal nonlinear delayed term driving the electronic feedback filter originates from the output intensity of the imbalanced fiber-based Mach-Zehnder interferometer:

$$|E|^2 = \gamma |E_0|^2 \cos^2\left[\frac{\omega_0 \delta T + \phi_T - \phi_{T+\delta T}}{2}\right], \qquad (1)$$

where ω_0 is the angular frequency of the laser light source and we have used the notation

$$\phi_T \equiv \phi(t - T). \qquad (2)$$

This quantity is detected by a broadband amplified photodetector. The latter performs both an optical intensity fluctuations conversion into the electrical domain $u \propto |E|^2$ and also a Fourier filtering according to the limited electronic bandwidth, which is generally smaller than the spectral broadening of the rf optical intensity fluctuations. This electrical signal is then linearly amplified by a broadband amplifier A, which is aimed at driving the rf input $v(t)$ of the PM with a potentially large amplitude, thus printing the optical phase modulation $\phi(t)$ on the light beam.

The limiting bandwidth is modeled by an electronic bandpass filter F characterized by two cutoff frequencies [$f_{\text{high}} = (2\pi\tau)^{-1}$ and $f_{\text{low}} = (2\pi\theta)^{-1}$; see Ref. [21]]. Using a simple second-order definition of the bandpass filter transfer function, an evolution equation for $x = \phi(t)/2 \propto v(t)$ can be derived

$$\frac{1}{\theta}\int_0^t x(\xi)d\xi + \tau\frac{dx}{dt} + x = \beta\begin{bmatrix}\cos^2\left(\frac{\omega_0\delta T}{2} + x_T - x_{T+\delta T}\right)\\ -\cos^2\left(\frac{\omega_0\delta T}{2}\right)\end{bmatrix}, \qquad (3)$$

where $\beta \propto \gamma|E_0|^2$ is practically adjusted through a variable optical attenuator changing γ. For mathematical clarity, we fix the offset phase at either $\omega_0\delta T = \pi/2$ or $-\pi/2$. Equation (3) then simplifies as

$$\theta^{-1}\int_0^t x(\xi)d\xi + \tau\frac{dx}{dt} + x = \pm\frac{\beta}{2}\sin[2(x_T - x_{T+\delta T})], \qquad (4)$$

where the plus and minus signs correspond to $\omega_0\delta T = -\pi/2$ and $\pi/2$, respectively. For those values of $\omega_0\delta T$ and by increasing β from zero, we note that the first Hopf bifurcation appears at its lowest possible value. This is explained by the Hopf bifurcation conditions. We note that $\omega_0 T$ only appears through a factor multiplying β [specifically, $\beta\sin(\omega_0\tau)$]. The minimal value of $|\beta|$ for a Hopf bifurcation then occurs if $|\sin(\omega_0\tau)| = 1$, meaning $\omega_0\delta T = \pm\pi/2$. Since we wish to observe a large number of higher-order bifurcations as we progressively increase β from zero, it is advantageous to start with a Hopf bifurcation exhibiting the lowest possible value.

Without loss of generality, we consider from now on

$$\omega_0\delta T = \pi/2 \qquad (5)$$

[minus sign in Eq. (4)] and $\beta > 0$. By introducing $u \equiv \int_0^t x(\xi)d\xi$, we may reformulate Eq. (4) as the following system of two coupled first-order delay-differential equations:

$$\tau\frac{dx}{dt} = -x - \frac{1}{\theta}u - \frac{\beta}{2}\sin[2(x_T - x_{T+\delta T})], \quad \frac{du}{dt} = x. \qquad (6)$$

IV. EIGENMODES

In order to find if pulsating instabilities are possible, we determine the Hopf bifurcations of the basic state $(x,u) = (0,0)$. From Eqs. (6) we formulate the linearized equations and look for a periodic solution of the form $x = a\exp(i\sigma s)$, where a is a constant and $s = t/\delta T$ is time normalized to the small delay. A nontrivial solution is possible if σ satisfies the characteristic equation

$$(1 + i\varepsilon_2\sigma)i\sigma + \varepsilon_1 + i\sigma\beta[e^{-i\sigma\zeta} - e^{-i\sigma(\zeta+1)}] = 0, \qquad (7)$$

where

$$\varepsilon_1 \equiv \delta T/\theta, \quad \varepsilon_2 \equiv \tau/\delta T, \qquad (8)$$

and

$$\zeta \equiv T/\delta T. \qquad (9)$$

Using the values of the experimental parameters θ, τ, T, and δT, we determine $\varepsilon_1 = 1.3\times10^{-4}$, $\varepsilon_2 = 5.1\times10^{-2}$, and $\zeta = 153.69$. The small values of ε_1 and ε_2 motivate the elimination of the terms multiplying ε_1 and ε_2. We then obtain from Eq. (7) a simple eigenvalue problem for σ given by

$$\exp[i\sigma(\zeta + 1/2)] = -2i\beta\sin(\sigma/2). \qquad (10)$$

From the real and imaginary parts, we obtain two conditions for β and σ,

$$\cos[\sigma(\zeta + 1/2)] = 0, \tag{11}$$

$$\sin[\sigma(\zeta + 1/2)] = -2\beta \sin(\sigma/2). \tag{12}$$

We concentrate only on the case $\sigma > 0$ [Eqs. (11) and (12) do not change if we replace σ by $-\sigma$]. Equation (11) determines the discrete frequencies σ of the time-periodic modes that are resonant with respect to the large delay T [from Eq. (9), ζ is T in units of δT]. Specifically, Eq. (11) is satisfied if

$$\sigma_p = \frac{\pi}{2\zeta + 1} + \frac{2p\pi}{2\zeta + 1}, \tag{13}$$

where the parity of p is imposed by the sign fulfillment in Eq. (12): An even mode is obtained with $p = 2n$ for $\sin(\sigma/2) < 0$ (e.g., σ close to π modulo 4π) or an odd mode with $p = 2n + 1$ when $\sin(\sigma/2) > 0$ (e.g., σ close to 3π modulo 4π). From Eq. (12) and using Eq. (13), we obtain the feedback gain β as

$$\beta_p = \frac{(-1)^{p+1}}{2\sin(\sigma_p/2)} > 0. \tag{14}$$

Figure 3(a) represents β_p as a function of σ_p. The solid line is provided by Eq. (14) and the red crosses reveal the discrete modes imposed by Eq. (13) (p is the upper horizontal axis). For clarity, we show in this figure only the $(2n + 1)$-odd modes close to $\sigma = \pi$. Equation (14) allows us to define a minimum gain eigenmode for which $|\sin(\sigma_p/2)|$ is necessarily close to 1. This occurs if σ_p is close to π modulo 4π (p odd) or if σ is close to 3π modulo 4π (p even). Therefore, this minimum gain condition is mathematically satisfied with multiple possible frequencies, but this degeneracy is usually removed experimentally in favor of the lowest frequency eigenmode. Indeed, the electronic amplifiers do not have an ideally flat frequency response over the full available frequency bandwidth covering many eigenmode frequencies. The gain profile in our experiment admits slightly more gain in the lower part of the electronic bandwidth pushing preferably the first eigenmode. This was already noted in Ref. [16], where a Hopf frequency shift was observed slightly below the theoretical minimum gain condition. Figure 3(b) illustrates this effect over several degenerate modes, through the successive parabolic dashed lines that exhibit progressively higher values of their minima. The red crosses denote the even modes already represented in Fig. 3(a) in the vicinity of $\sigma = \pi$ and the figure also indicates the other degenerate modes: odd ones around 3π (blue dots) and even ones around 5π (red crosses).

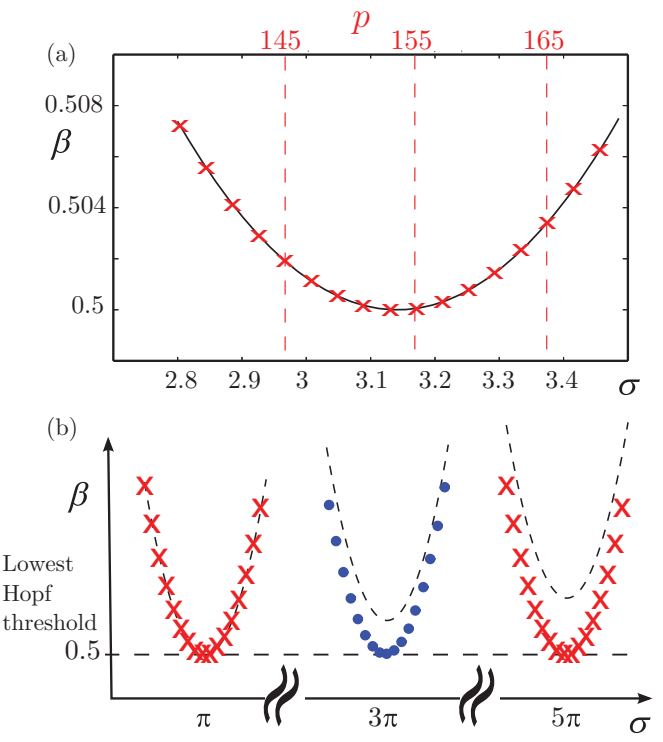

FIG. 3. (Color online) Each cross represents a Hopf bifurcation point located at $\beta = \beta_p$ and characterized by a frequency $\sigma = \sigma_p$. Because of Eq. (5), the first Hopf bifurcation occurs at its minimal possible value ($\beta = 1/2$). (a) Crosses satisfy Eqs. (11) and (12) with $\zeta \simeq 153.69$, i.e., σ in the vicinity of π. (b) Degenerate modes with the odd and even modes alternated every 2π. As explained in the text, the mode degeneracy is removed by the nonflat electronic gain and is illustrated by the dashed parabola, implying an actually higher Hopf threshold for the high-frequency modes.

V. PRIMARY BIFURCATION

We wish to determine an asymptotic approximation of the bifurcation points (13) and (14) that are valid in the limit $\zeta \to \infty$. To this end, we expand the parameters ζ as

$$\zeta = \varepsilon^{-1} + a_0 + \varepsilon a_1 + \cdots, \tag{15}$$

where

$$\varepsilon \equiv p^{-1} = \frac{1}{2n} \tag{16}$$

is a small parameter, with $p = 2n$ a large fixed integer determined from Eq. (13) with the constraint $\sigma \simeq \pi$, as explained in the preceding section [21]. We next seek a solution for (σ,β) close to $(\pi,1/2)$ of the form

$$\sigma = \pi + \varepsilon\sigma_1 + \varepsilon^2\sigma_2 + \cdots, \tag{17}$$

$$\beta = \tfrac{1}{2} + \varepsilon\beta_1 + \varepsilon^2\beta_2 + \cdots. \tag{18}$$

Inserting Eqs. (15), (17), and (18) into Eqs. (13) and (14), we equate to zero the coefficients of each power of ε. We obtain a sequence of problems for the unknown coefficients $\sigma_1,\sigma_2,\beta_1,\beta_2,\ldots$, from which we find

$$\sigma_1 = -\pi a_0,$$
$$\sigma_2 = \pi\left[-a_1 + \frac{a_0}{2}(2a_0 + 1)\right], \tag{19}$$
$$\beta_1 = 0, \quad \beta_2 = \frac{\sigma_1^2}{16}.$$

The first primary Hopf bifurcation that marks the change of stability of the basic steady state corresponds to the lowest value of β_2. The fact that the leading approximation of the Hopf frequency is π suggests a bifurcation to 2-periodic square-wave oscillations in units of time s. Note that the period is not exactly 2 but admits a correction that depends on a_0: using

Eq. (17), the period $2P$ is given by

$$2P \equiv \frac{2\pi}{\sigma} = 2(1+\varepsilon a_0) + O(\varepsilon^2). \tag{20}$$

We next consider the full nonlinear problem. Motivated by the linearized theory indicating a first Hopf bifurcation with period 2 in units of

$$s = t/\delta T, \tag{21}$$

we rewrite Eq. (6) in terms of s and with the variable $u \equiv \delta T y$ and obtain

$$\varepsilon_2 \frac{dx}{ds} = -x - \varepsilon_1 y - \frac{\beta}{2}\sin[2x_\zeta - 2x_{\zeta+1}], \tag{22}$$

$$\frac{dy}{ds} = x. \tag{23}$$

From our analysis of the Hopf bifurcation points, we anticipate a first Hopf bifurcation close to $\beta = \beta_H = 1/2$, leading to $2P$-periodic square-wave oscillations with $2P$ defined by Eq. (20). As for the analysis of the Hopf bifurcation conditions, we neglect the contributions of ε_2 and ε_1 and expect to formulate a simpler problem. We have verified numerically that their elimination does not affect the bifurcation diagram provided we limit our attention to the first bifurcations located in the prechaotic region. Setting $\varepsilon_1 = \varepsilon_2 = 0$, Eq. (22) reduces to a single equation for x given by

$$x(s) = -\frac{\beta}{2}\sin[2x_\zeta - 2x_{\zeta+1}]. \tag{24}$$

This equation defines a map that relates $x(s)$ to x_ζ and $x_{\zeta+1}$. We next plan to reformulate it by taking advantage of the large value of ζ and its particular relation with the half period P . To this end, we simply calculate the ratio ζ/P using Eqs. (15) and (20) and obtain

$$\frac{\zeta}{P} = p + O(\varepsilon), \tag{25}$$

i.e., an exact integer ratio as $\varepsilon \to 0$. Consequently, the expressions of x_ζ and $x_{\zeta+1}$ in Eq. (24) can be rewritten as $x_\zeta = x_{pP} + O(\varepsilon)$ and $x_{\zeta+1} = x_{(p+1)P} + O(\varepsilon)$. Equation (24) then becomes

$$x(s) = -\frac{\beta}{2}\sin[2(x_{pP} - x_{(p+1)P})] + O(\varepsilon). \tag{26}$$

With the notation

$$x_k \equiv x(s), \quad x_{k-1} \equiv x_P, \tag{27}$$

Eq. (26) admits the compact form

$$x_k = -\frac{\beta}{2}\sin[2x_{k-p} - 2x_{k-p-1}]. \tag{28}$$

In order to determine the Hopf bifurcation branch, we seek a 2-periodic fixed point of Eq. (28) satisfying the condition $x_k = x_{k-2}$. Two successive iterations of Eq. (28) provide two equations for the extrema $u_0 = x_k$ and $u_1 = x_{k-1}$,

$$u_0 = -\frac{\beta}{2}\sin(2u_1 - 2u_0), \tag{29}$$

$$u_1 = -\frac{\beta}{2}\sin(2u_0 - 2u_1), \tag{30}$$

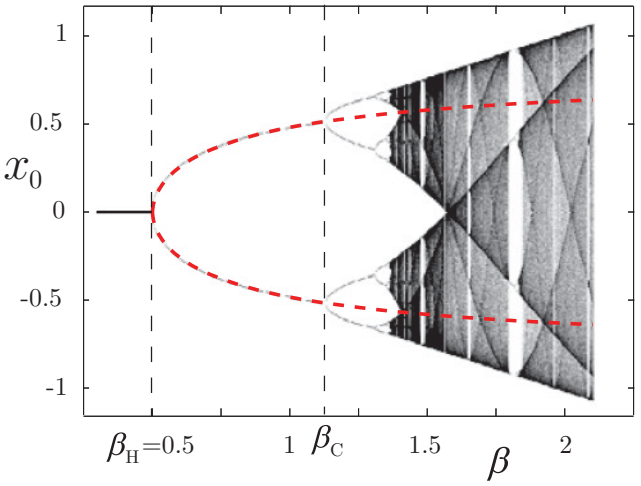

FIG. 4. (Color online) Numerical bifurcation diagram. The dashed red curve corresponds to the extrema u_0 and u_1 of the basic square-wave period-2 solution, from Eq. (29). The grayscale dots denote vertically the extrema probability for the corresponding bifurcation parameter, calculated from the asymptotic dynamic of the sine map in Eq. (38).

which imply that $u_1 = -u_0$ and

$$u_0 = \frac{\beta}{2}\sin(4u_0). \tag{31}$$

The branch of $2P$-periodic solutions emerging from the first Hopf bifurcation is shown by a thick red dashed line in Fig. 4. It is obtained from the parametric solution $\beta = 2u_0/\sin(4u_0)$ and $u_1 = -u_0$. This solution represents our basic primary branch that connects the first Hopf bifurcation of the steady state. We are now ready to determine higher-order bifurcations. Note that the basic dimensionless time s implies that the period of the square-wave oscillations in units of time t is

$$T_1 = 2P\delta T = 2\delta T + O(\varepsilon), \tag{32}$$

as the experiments suggested.

VI. SECONDARY BIFURCATION

As indicated by the experiments, we now assume that the Hopf bifurcation branch undergoes a secondary bifurcation to a slowly modulated, fast $2P$-periodic square-wave oscillations. Specifically, we seek a solution that depends on both time s (t normalized to δT) and the slower time

$$\rho \equiv \varepsilon s. \tag{33}$$

We apply the method of multiple time scales [22–24]. The assumption of two independent time variables implies the chain rules

$$x_\zeta = x(s - \zeta, \rho - 1 + O(\varepsilon)), \tag{34}$$

$$x_{\zeta+1} = x(s - \zeta - 1, \rho - 1 + O(\varepsilon)). \tag{35}$$

Instead of Eqs. (26) and (24) now becomes

$$x(s,\rho) = -\frac{\beta}{2}\sin\begin{bmatrix} 2x(s - pP, \rho - 1) \\ -2x(s - (p+1)P, \rho - 1) \end{bmatrix} + O(\varepsilon). \tag{36}$$

We proceed as for Eq. (26). The leading approximation as $\varepsilon \to 0$ is the equation for the map

$$x_k(\rho) = -\frac{\beta}{2}\sin[2x_{k-p}(\rho-1) - 2x_{k-p-1}(\rho-1)]. \quad (37)$$

Similarly to the derivation of Eq. (31), we look for a 2-periodic fixed point of Eq. (37) satisfying the condition $x_k = x_{k-2}$. The extrema $u_0 = x_k$ and $u_1 = x_{k+1}$ now satisfy the conditions $u_1 = -u_0$ and

$$u_0(\rho) = \frac{\beta}{2}\sin[4u_0(\rho-1)]. \quad (38)$$

Equation (38) is equivalent to the well-known sine map $v_{j+1} = r\sin(\pi v_j)$ with $u_0(\rho) = \pi v_{j+1}/4$, $u_0(\rho-1) = \pi v_j$, and $r = 2\beta/\pi$ [25]. Equation (38) describes the long time modulation effects of the rapid $2P$-periodic square-wave oscillations. Its period-1 fixed point satisfies the condition $u_0(\rho-1) = u_0$ and Eq. (38) reduces to Eq. (31), as expected. We already know that it corresponds to the fast $2P$-periodic square-wave oscillations in units of time s; however, Eq. (38) admits other fixed points (see Fig. 4) that gradually lead to chaotic oscillations as β increases. This is exactly what we have observed experimentally. The crenelated envelope of the rapid oscillations shown in Fig. 1(e) occurs for $\beta = 1.14$, which corresponds to the domain $\beta_C \simeq 1.13 < \beta < 1.31$ of the secondary bifurcation to a period-2 fixed point of Eq. (38), as shown in Fig. 4. The period of the crenelated oscillations corresponding to this period-2 fixed point is, using Eq. (33), equal to $T_2 = 2\varepsilon^{-1}$ in units of time s. Using then the definition of s and Eq. (15), the period in real units of time t is

$$T_2 = 2\delta T\varepsilon^{-1} \simeq 2p\delta T \simeq 2T, \quad (39)$$

where p is a large integer. As β is increased further, higher-order bifurcations appear following the period-doubling route to chaos of the sine map.

VII. CONCLUSION

We have studied experimentally and analytically the first instabilities in a nonlinear double-delay electro-optic phase oscillator. Although the system is modeled by a second-order coupled delay-differential equation, an asymptotic approximation based on a strong separation of the delay times leads to a successful description of the first bifurcations observed as the feedback gain increases. Our analysis highlights the dominating modal competition imposed by the delay times and their resonant conditions.

We showed that the bifurcation diagram exhibits a cascade of bifurcations to multiperiodic regimes characterized by fast $T_1 \simeq 2\delta T$ oscillations modulated by crenelated envelopes with periods that are multiples of $T_2 \simeq 2p\delta T$. Note that the ratio $T_2/T_1 \simeq p$ is a large integer, which explains why the overall oscillations appear nearly periodic over long intervals of time. Our results suggest a secondary bifurcation to a periodic state (periodic locking) rather than a torus bifurcation exhibiting two incommensurable frequencies. However, a different analysis is needed to explore the nature of this secondary bifurcation. The successive bifurcation transitions are elegantly described by the sine map (38), which depends only on the two delays. We have verified numerically by simulating the original equations that the limiting bandwidth of the electronics does not play a role on the bifurcation diagram in the first approximation (the parameters ε_1 and ε_2 have been neglected). It is involved at the level of the mode selection between the discrete modes exhibiting equal or very similar gain thresholds and is determinant if we are interested in describing the fast transition layers between flat plateaus. Moreover, these transition layers certainly needs to be taken into account for the higher-order bifurcations and chaotic regimes where strongly pulsating oscillations are observed. At moderate values of the feedback gain β, we could accurately describe theoretically the occurrence of the crenelated fast oscillations that result from the fact that we have two distinct time scales parametrized by the two delays T and δT. The fact that the fast periodic oscillations are square-wave oscillations does not play a role. In Refs. [26,27] crenelated slowly varying envelopes modulate fast pure sine oscillations. The EOO in these other publications involve only one delayed feedback and the delay is large compared to the basic time of the fast oscillations.

[1] T. Erneux, *Applied Delay Differential Equations* (Springer, Berlin, 2009).

[2] *Delay Differential Equations, Recent Advances and New Directions*, edited by A. Balachandran, T. Kamár-Nagy, and D. E. Gilsinn (Springer, Berlin, 2009).

[3] G. Stepan, in Special issue of Philos. Trans. R. Soc. A **367**, 1059 (2009).

[4] F. M. Atay, *Complex Time-Delay Systems* (Springer, Berlin, 2010).

[5] W. Just, A. Pelster, M. Schanz, and E. Schöll, in Special issue of Philos. Trans. R. Soc A **368**, 303 (2010).

[6] Special issue on *Time Delay Systems*, edited by T. Kalmá Nagy, N. Olgac, and G. Stépán, J. Vib. Control **16**(6/7) (2010).

[7] M. Lakshmanan and D. V. Senthilkumar, *Dynamics of Nonlinear Time-Delay Systems*, Springer Series in Synergetics, Vol. 1 (Springer, Berlin, 2010).

[8] Hal Smith, *An Introduction to Delay Differential Equations with Applications to the Life Sciences*, Texts in Applied Mathematics, Vol. 57 (Springer, Berlin, 2010).

[9] T. Erneux and P. Glorieux, *Laser Dynamics* (Cambridge University Press, Cambridge, 2010).

[10] A. Argyris, D. Syvridis, L. Larger, V. Annovazzi-Lodi, P. Colet, I. Fischer, J. Garcia-Ojalvo, C. R. Mirasso, L. Pesquera, and K. A. Shore, Nature (London) **438**, 343 (2005).

[11] A. Uchida, K. Amano, M. Inoue, K. Hirano, S. Naito, H. Someya, I. Oowada, T. Kurashige, M. Shiki, S. Yoshimori, K. Yoshimura, and P. Davis, Nature Photon. **2**, 728 (2008).

[12] B. Mensour and A. Longtin, Phys. Rev. E **58**, 410 (1998).

[13] A. Ahlborn and U. Parlitz, Phys. Rev. Lett. **93**, 264101 (2004); Phys. Rev. E **72**, 016206 (2005).
[14] C. Marriott, R. Vallée, and C. Delisle, Phys. Rev. A **40**, 3420 (1989).
[15] M. W. Lee, L. Larger, V. S. Udaltsov, É. Genin, and J.-P. Goedgebuer, Opt. Lett. **29**, 325 (2004).
[16] R. Lavrov, M. Peil, M. Jacquot, L. Larger, V. Udaltsov, and J. Dudley, Phys. Rev. E **80**, 026207 (2009).
[17] J. Lasri, P. Devgan, R. Tang, and P. Kumar, Opt. Express **11**, 1430 (2003); IEEE Photon. Technol. Lett. **16**, 263 (2004).
[18] Y. Kouomou Chembo, A. Hmima, P.-A. Lacourt, L. Larger, and J. M. Dudley, J. Lightwave Technol. **27**, 5160 (2009).
[19] L. Larger and J.-P. Goedgebuer, C. R. Phys. **5**, 609 (2004).
[20] R. Lavrov, M. Jacquot, and L. Larger, IEEE J. Quantum Electron. **46**, 1430 (2010).
[21] The values of the fixed parameters are $\theta = 5.3$ μs, $\tau = 20.7$ ps, $T = 61.89$ ns, and $\delta T = 402.68$ ps. This leads to $\zeta = 153.67$, and therefore $\varepsilon = 0.0065$, and $a_0 = 0.67$.
[22] C. M. Bender and S. A. Orszag, *Advanced Mathematical Methods for Scientists and Engineers* (McGraw Hill, New York, 1978).
[23] J. Kevorkian and J. D. Cole, *Multiple Scale and Singular Perturbation Methods* (Springer, Berlin, 1996).
[24] F. Verhulst, *Methods and Applications of Singular Perturbations: Boundary Layers and Multiple Timescale Dynamics* (Springer, Berlin, 2005).
[25] S. H. Strogatz, in *Nonlinear Dynamics and Chaos* (Addison-Wesley, Reading, MA, 1995), p. 369.
[26] Y. Kouomou Chembo, L. Larger, H. Tavernier, R. Bendoula, E. Rubiola, and P. Colet, Opt. Lett. **32**, 2571 (2007).
[27] Y. Chembo, L. Larger, and P. Colet, IEEE J. Quantum Electron. **44**, 858 (2008).